Metall. Res. Technol. **112**, 605 (2015)

DOI: 10.1051/metal/2015039
www.metallurgical-research.org

&Metallurgical Research Technology

Application study of AlSi10Mg alloy by selective laser melting: physical and mechanical properties, microstructure, heat treatments and manufacturing of aluminium metallic matrix composite (MMC)

Arnold Mauduit, Sébastien Pillot and François Frascati

CETIM CERTEC (CRAl: centre de référence de l'aluminium, Pole matériaux et procédés), 9 Boulevard Lahitolle, 18000 Bourges, France
e-mail: arnold.mauduit@cetim-certec.com

Key words:
Selective laser melting; AlSi10Mg; MMC; SiC; microstructure; heat treatments; physical and mechanical properties

Abstract – Samples of AlSi10Mg alloy were first constructed, selecting the manufacturing parameters through a parametric method based on an experimental design; with the same technique, samples of a metallic matrix composite (AlSi10Mg matrix base and particles of SiC reinforcements) were also made. The evolution of the density with the introduction of reinforcements into the AlSi10Mg alloy was studied. This showed an increase in the porosity level with the reinforcement volume fraction. The material hardness and electrical conductivity were then evaluated, along with conventional mechanical characteristics, and microstructural changes with respect to heat treatments on both the AlSi10Mg alloy material and AlSi10Mg matrix composite. Doing so allows correlating material hardness and electrical conductivity (as observed for conventionally produced alloys: casting or wrought). The tensile strength, yield strength and Young's modulus were measured. A significant increase in the conventional mechanical characteristics compared with casting was shown, due to hardening by structure refinement. Evidence is given to relate the yield strength value to the reduction in the dendrite arm spacing (DAS) by application of the Hall-Petch law. We discuss the understanding of the thermal process involved (temperature distribution and fast cooling rate). In addition, observations and analysis of the microstructural changes are presented: building tracks, the disturbed zone, and structural variations linked to heat treatment.

Received 9 March 2015
Accepted 24 September 2015

Selective laser melting (SLM) is an additive manufacturing method, the latter designating all industrial processes allowing the direct manufacturing of functional components. It is defined by the layer-by-layer construction of the desired component: a laser fuses metal powder following 3D data input from a computer. This technology offers great advantages thanks to its rapid process, the absence of tooling (e.g. moulds), fewer production constraints during the design stage, potential mass gains, etc.

Aluminium alloys are not often employed with this technique. Indeed, these appear ill-suited, mainly due to the natural layer of oxide generated on the material surface, but also due to their high reflectivity (of the laser beam) and their thermal conductivity. Nevertheless, the potential gains of selective laser melting of aluminium alloy may be studied from an industrial component production point of view. Particularly for metal matrix composites, it allows a finished component with little to no need for machining so as to reduce extra costs related to tool wear (for example).

Thus, in this document we study samples of AlSi10Mg aluminium alloy and MMCs (AlSi10Mg matrix base with SiC reinforcements) obtained by SLM in order to observe and explain some mechanical and

Fig. 1. Selective laser melting machine – Phenix Systems PM100 – 200 W.

metallurgical properties of these materials (density, metallurgical structure, heat treatments, mechanical characteristics, etc.).

1 Material and method

1.1 Selective laser melting machine

The machine used in this study was a Phenix Systems PM 100 equipped with a 200 W fibre laser YAG (Fig. 1).

The building platforms of parts and samples are made of aluminium alloy. The temperature within the processing chamber was set to 200 °C. All trials were performed with a protective atmosphere (pure argon – min 99.99%) to prevent oxidation of the aluminium alloy (AlSi10Mg); the layer thickness was set to 30 μm. The manufacturing strategy influences the properties of fabricated parts. Several manufacturing strategies exist and our choice is known as "crossed" (Fig. 2). In this strategy, tracks built in the same plane all have the same orientation. The execution order of the tracks is shown in Figure 2 (order of lasing). The direction of the laser beam (and therefore the tracks) is alternated. The square in Figure 2 indicates the direction of manufacturing tracks (first layer with a red arrow, f ollowed by the second with a green arrow), hence the term "crossed" strategy.

1.2 AlSi10Mg alloy – powder and mixing

This alloy is primarily used for moulding. The main chemical elements are: about 10% (mass) silicon (Si), 0.35% (mass) magnesium (Mg) and iron (Fe). Several secondary elements may be accounted for, such as nickel (Ni), zinc (Zn) and titanium (Ti). The level of silicon brings the alloy composition close to eutectic for this family, thus providing it with excellent casting properties (particularly good castability). The magnesium content allows heat-treating the material (Technique de l'ingénieur M4675 [1]).

For over a decade, this alloy has been used for laser additive manufacturing with varying success: it was among the first to be supplied as powder (industrially). The knowledge (in SLM), the availability and the good castability of this alloy are the reasons why we used it as a matrix for the composite (MMC).

The AlSi10Mg alloy used in this study was provided by TLS Technik with the following characteristics:

- Powder: spherical particles.
- d_{90} = 32 μm – d_{50} = 18 μm.

Metal matrix composites are a composite material made of a metal matrix with reinforcements, either metallic or ceramic. They are commonly referred to as MMCs.

The aluminium metal matrix composites studied were formed by:

- An aluminium matrix of AlSi10Mg (see above).
- SiC reinforcements (angular particles – d_{90} = 13.7 μm and d_{50} = 5 μm). The density of the SiC is 3210 kg.m^{-3}.

The following designation is henceforth used in this study for aluminium MMCs:

Alloy/reinforcement/volume fraction form (particles p or fibres f) – temper.

For example: AlSi10Mg/SiC/10p – T6.

1.3 Samples

Small pins or cylinders (Fig. 3) were manufactured from the AlSi10Mg alloy and MMCs of the following dimensions:

- Diameter 10 mm.

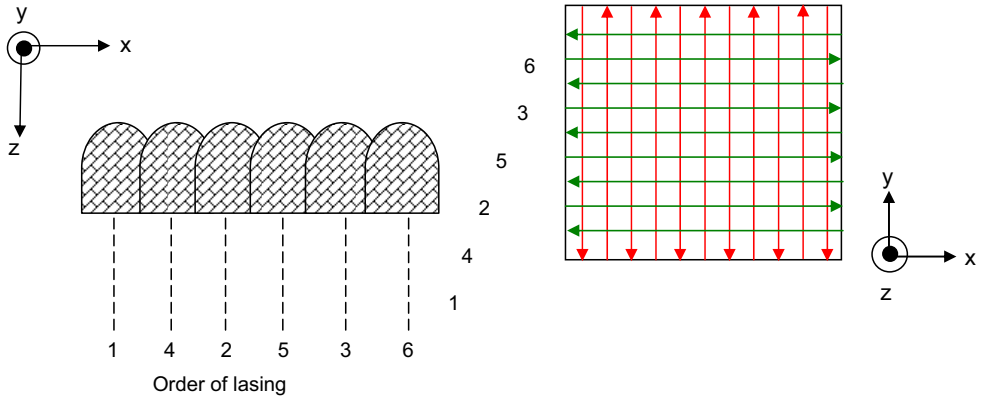

Fig. 2. "Crossed" manufacturing strategy.

Fig. 3. Pin sample of AlSi10Mg alloy.

– Height 10 mm.

These pins are mainly used for heat treatments, metallographic study, density control, and hardness and electrical conductivity checks.

Cylindrical tensile test samples were manufactured horizontally (in plane (x, y)) and vertically (Z-direction). The test samples were then drilled to the required final geometry according to ISO 6892 [2] (Fig. 4).

Rectangular samples were also produced and further machined (approximately $80 \times 10 \times 2.5$ mm) for evaluation of Young's modulus through vibratory testing.

1.4 Heat treatment: heating and cooling procedures

An oven with forced air convection was used for heat treatments. It is specifically designed for treating aluminium alloys (temperatures ≤650 °C) and is characterised by excellent temperature homogeneity ($\Delta T \leq 6$ °C). The hardening fluid used was cold water (≈20 °C). The transfer time of the samples in the hardening area was in all cases under 10 s (according to SAE AMS2772E [3]).

The heat treatments on the AlSi10Mg alloy and the MMCs generated by selective laser melting were:

– Artificial ageing at 160 °C for 1 h, 5 h or 10 h.
– Solution treatment at 540 °C for 1 h or 3 h followed either by natural ageing or artificial ageing at 160 °C for 5 h.

1.5 Archimedes method

The Archimedes method allows determining the overall porosity of a sample,

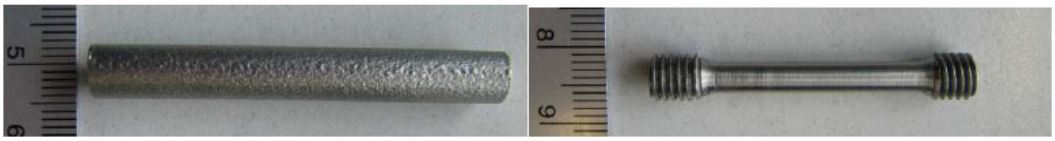

Fig. 4. Cylindrical samples (length = 60 mm – diameter = 10 mm) and reduced tensile samples ($L_0 = 5.65\sqrt{S_0} = 25$ mm with S_0 cross-section).

differentiating the open porosity P_o from the closed porosity P_f. This method is often used to determine the density of parts and samples made by SLM [4].

The principle is to measure mass m_1 in air and mass m_3 in liquid, to which we add a measurement in air of mass m_2 of the sample, which has been impregnated with the wetting fluid (distilled water).

Let m_1 be the dry sample mass in air (g).
Let m_2 be the wet sample mass in air (g).
Let m_3 be the immersed sample mass in water (g).
Let ρ_{liq} be the water density.
Let ρ_{th} be the theoretical density of the evaluated material.
P_o and P_f may be expressed (in %) as follows:

$$P_o = \frac{m_2 - m_1}{m_2 - m_3} \times 100 \quad (1)$$

$$P_f = \frac{m_1\left(1 - \frac{\rho_{liq}}{\rho_{th}}\right) - m_3}{m_2 - m_3} \times 100 \quad (2)$$

1.6 Mechanical tests (tensile testing)

Tensile testing trials were conducted at ambient temperature and at 180 °C, pursuant to NF EN ISO 6892-1 and -2 [2] on a 100 kN W&B LFM machine (accuracy class 0.5 – range 1–100 kN). The tensile test speed used was 5 mm.min^{-1}.

1.7 Vibratory tests (Young's Modulus *E*)

Vibratory tests were performed to determine the Young's modulus of the studied materials. They are based on the resonance of a uniform beam in planar flexion. Vibratory evaluation consists of applying a known stress to the beam, then measuring its response. Simple geometrical constructions such as beams (Sect. 2.3) are used with known boundary conditions. Under these conditions, it is possible to extract a value for E (Young's modulus) from the natural frequency.

For a beam of rectangular cross-section, the equation is given by (Oberst's method [5]):

$$E = \frac{\mu}{I}\left(\frac{2\,\pi\, fi\, L^2}{Ai}\right)^2 \quad (3)$$

with:

- E: Young's modulus;
- i: the subscript referring to the modal number of the vibratory mode (here $i = 1$, the first mode of vibration);
- fi: the natural frequency for said mode in Hz (here f1);
- L: the beam length in m;
- μ: the linear mass of the beam in kg.m^{-1};
- I: moment of inertia in m^4;
- Ai: a coefficient related to the vibratory mode and the boundary conditions (here $A1$: free-free – first mode of vibration => $A1 = 22.4$).

1.8 Hardness and electrical conductivity trials

These tests were conducted at ambient temperature such that:

- For Brinell hardness and Vickers microhardness: Struers Duramin 500/A300 machines (according to NF EN ISO 6506-1 [6] and 6507-1 [7]) were used. A minimum of three measurements per sample were performed.
- For electrical conductivity: a Fischerscope MMS device (without temperature adjustment) was used. Trials were performed at 21 ± 2 °C, with a minimum of three measurements per sample.

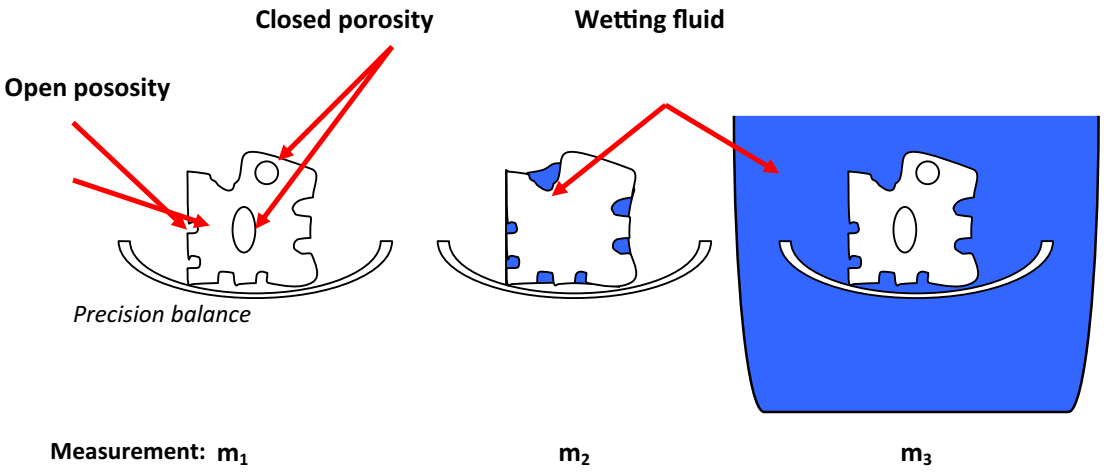

Fig. 5. Basis of the Archimedes method.

Table 1. Manufacturing parameters.

Alloys	Power (W)	Speed ($mm.s^{-1}$)	Coverage indicator (%)	Compacting indicator (%)
AlSi10Mg or AlSi10Mg/SiC/0p	200	700	60	50
AlSi10Mg/SiC/5p	200	560	52	100
AlSi10Mg/SiC/10p	200	800	54	87.5
AlSi10Mg/SiC/15p	200	700	60	50

1.9 Micrographic examination and SEM

Samples for micrographic evaluation were conventionally prepared (cutting, mounting, polishing, micrographic etching, etc.) prior to observation under an optical microscope Zeiss Axio imager M2m. For information purposes, two types of etching were used: reagent with sulphuric acid (10% H_2SO_4 and 5% HF) and Barker's reagent (electrolytic etching with processing parameters: 30 V – 1 min).

Similarly, samples for Scanning Electron Microscopy (SEM) were prepared in the usual fashion and observed under a SEM Zeiss EVD. The latter is equipped with an EDS (Energy Dispersive X-ray Spectroscopy) sensor.

2 Results and discussion

2.1 Preliminary results

The objective was to determine an optimum SLM processing window for the AlSi10Mg alloy and the corresponding MMCs.

Three main processing parameters (factors for a DOE) were selected:

- the laser scan velocity, noted V;
- the recovery rate between two beam paths, Tr which is directly related to the scan spacing, E_v (the scan spacing being the distance between two consecutive laser beams);
- and the compacting indicator T_c (the compacting indicator being the percentage of the layer thickness deposited in excess of said thickness, e.g. a T_c of 50% for a layer of 30 μm gives a thickness of deposited powder of 45 μm).

Too low or too high values for these factors lead to decreased densification, and hence poor mechanical properties of the manufactured components.

We could use a Box Behnken experimental design (DOE) to meet our needs: one DOE per material. The output of this DOE is the closed porosity using the Archimedes method. The open porosity was not kept as a selection criterion, given the high measurement uncertainties related to the mass evaluation of water-impregnated samples.

Table 1 summarises the main parameters of interest for manufacturing of samples in AlSi10Mg alloy and the various MMCs studied.

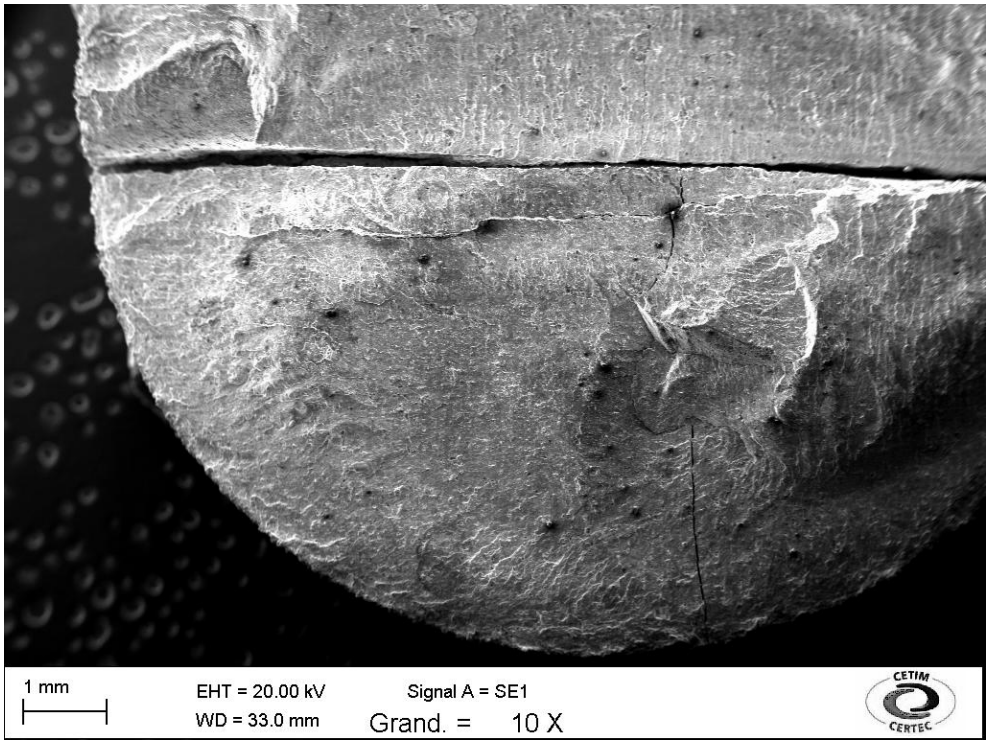

Fig. 6. Pin sample cracking (AlSi10Mg/SiC/15p – as built).

The volume fraction of SiC in the MMCs presented here is limited to 15%. Indeed, usable samples (even pins) are harder to obtain for higher fractions. As shown in Figure 6, the samples are cracked; this phenomenon is enhanced with increased SiC volume fractions. Cracking is possibly due to internal stresses induced by the manufacturing method.

2.2 Characterisation

2.2.1 Sample density

Note that the theoretical density for AlSi10Mg alloy, based on the chemical composition of the material batch used (see Sect. 2.2.2, Table 2) for the study is 2654 kg.m^{-3}.

The pins retained for the study have a density ranging from 2630 to 2650 kg.m^{-3}, i.e. very close to the theoretical volume mass of the AlSi10Mg alloy batch studied. On average, the density of the samples made of AlSi10Mg alloy is 2641 kg.m^{-3}.

From Figure 7a, it is clear that despite the inclusion of SiC reinforcements and a higher density than aluminium, the composite densities remain lower than that of the alloy alone. This is simply due to increased porosity. The insertion of reinforcements into an aluminium metal matrix is therefore generally detrimental to porosity.

Nevertheless, the composites density grows linearly with the reinforcements (SiC) volume fraction, as per Figure 7b. Since this measured curve is not parallel to its theoretical counterpart (magenta line on Fig. 7a), it appears there is a linear relationship between the porosity and reinforcements volume fraction.

2.2.2 Chemical analysis

Chemical analysis following the ICP-AES method was conducted on the AlSi10Mg powder supplied by TLS Technik (Table 2). It appears the chemical compound Mg is above the tolerance limits: 0.75% (mass) instead of 0.45% (mass) for the standard composition of AlSi10Mg (according to NF EN 1706 [8]). A second analysis was performed (Table 2) on a "pin" sample of AlSi10Mg manufactured using SLM (see Sect. 1.3).

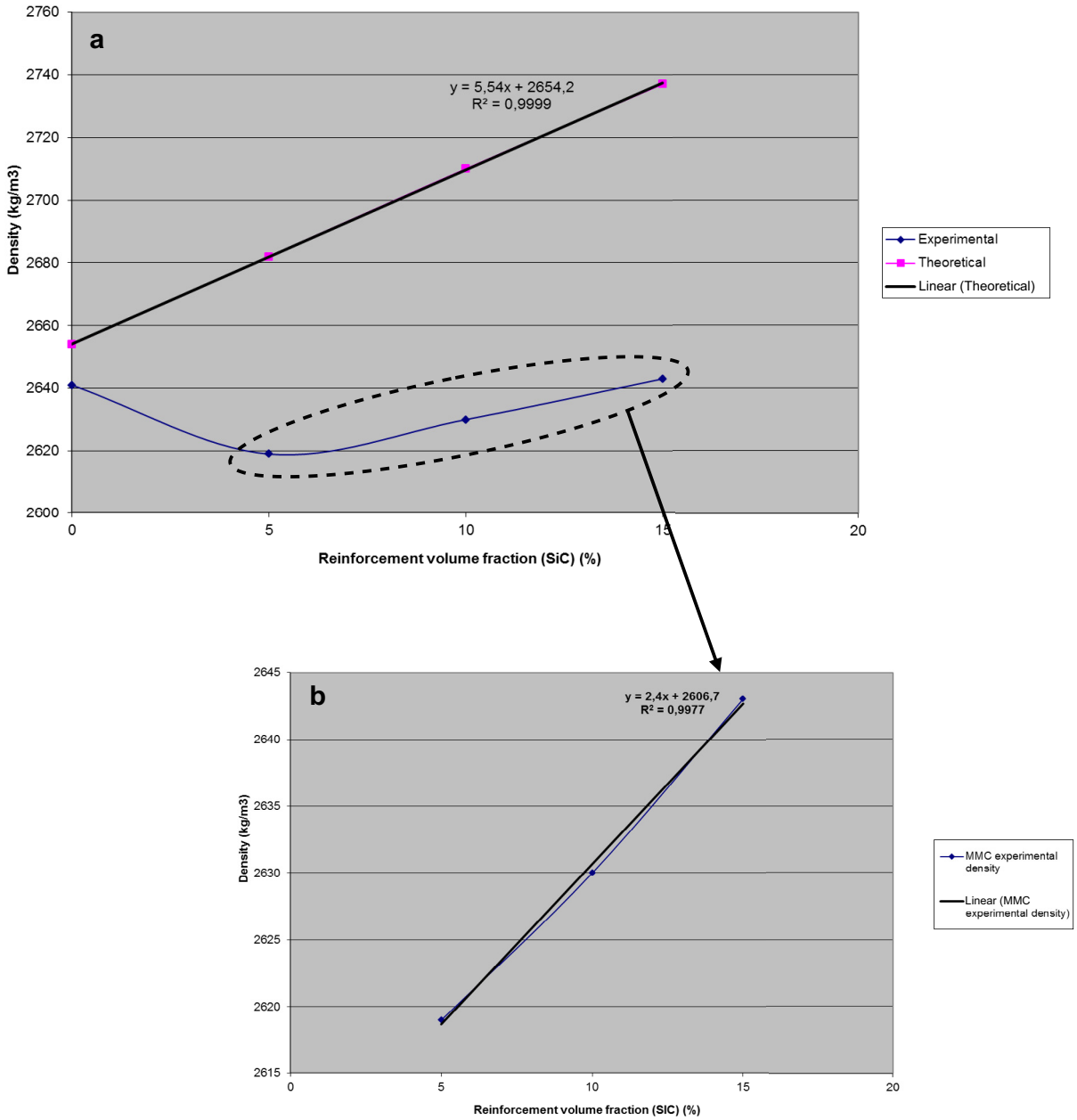

Fig. 7. (a) Average density related to the reinforcement volume fraction. (b) Composites average density model.

Table 2. Chemical analysis (Wt%) of the powder and a AlSi10Mg alloy pin made by selective laser melting.

AlSi10Mg	Si	Fe	Cu	Mn	Mg	Cr	Ni	Zn	Ti
Powder	10.1	0.19	<0.005	<0.005	0.75	0.007	0.009	0.008	0.014
Pin	10.6	0.16	<0.005	<0.005	0.32	0.005	0.007	0.008	0.009
Standard Table 1 NF EN 1706	9.0 to 11.0	0.55	0.10	0.45	0.20 to 0.45	–	0.05	0.10	0.15

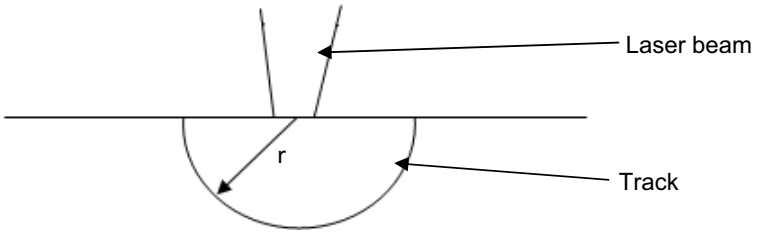

Fig. 8. Simplified modelling of a track.

The results show the compound Mg has decreased to 0.32% (mass), which is fully compliant with the standard composition of AlSi10Mg.

Thus, there is a 0.43% loss of Mg. The latter has the lowest vaporisation temperature (1090 °C) amongst all other compounds present; it is thus possible that part of the magnesium vaporised during the laser fusion process. This phenomenon was also observed at the LERMPS laboratory [9]. Powders are thus supplied with an increased quantity of magnesium to ensure the conformity (according to NF EN 1706 [8]) of the alloy after selective laser melting.

According to Tissot [10], with a simple modelling of a track with a hemispherical melt (Fig. 8) which is quite close to reality (see Fig. 22), it is possible to determine the theoretical maximum temperature difference in the track from Equation (4):

$$\Delta T = \frac{q}{2\,\lambda\,\pi\,r} \tag{4}$$

with:

q: power passing through the surface of the melt bath. q = 40 W, allowing the power transmitted to the track to be 20% (estimation) of the laser power (200 W); this is due to the high reflectivity of the aluminium alloy [11].

λ: thermal conductivity of the AlSi10Mg alloy made by SLM. λ = 103 W.m^{-1}.°C^{-1} [12].

r: mean radius of the track. r = 78 μm because the average width of the tracks was evaluated as being 156 μm in the DOE.

Thus, under these conditions, an evaluation of ΔT is 792 °C. Assuming that the contour of the track is 600 °C (the liquidus temperature for this AlSi10Mg alloy), then the maximum temperature at the centre of the laser beam is 1392 °C, which is greater than 1090 °C magnesium evaporation.

2.2.3 Hardness and electrical conductivity

Figure 9 below shows the evolution of microhardness HV0.3 and hardness HBW 1/10 with respect to the artificial ageing duration: base (no tempering, 0 h), 1 h of artificial ageing at 160 °C, 5 h of artificial ageing at 160 °C and 10 h of artificial ageing at 160 °C for the AlSi10Mg alloy. Both these hardnesses (micro/macro) are used to evaluate the potential influence of porosity on hardness measurements.

There are no notable differences in the behaviour of either hardness: conclusions will thus be identical for both. As such, only the HBW 1/10 results will be discussed hereafter. Artificial ageing has little influence on the as-built temper, regardless of the hardness. The slight decrease in the alloy hardness after artificial ageing for 10 h at 160 °C is most probably related to the higher porosity of the sample pin (0.7% against 0.1% closed porosity for all other pins) rather than evidence of the influence of the artificial ageing.

Figure 10 describes the influence of conventional heat treatments, i.e. solution heat treatment, quenching, and natural or artificial ageing, so as to obtain temper T4 and T6, on the HBW 1/10 hardness of pins manufactured by selective laser melting (AlSi10Mg alloy and MMCs).

All hardness values (for all natural and artificial ageing cases) are lower than those obtained from as built temper. As expected, the hardness of T4 is lower than that of T6.

The values obtained in this study were also compared with normalising values found in the literature, as given in Table 3.

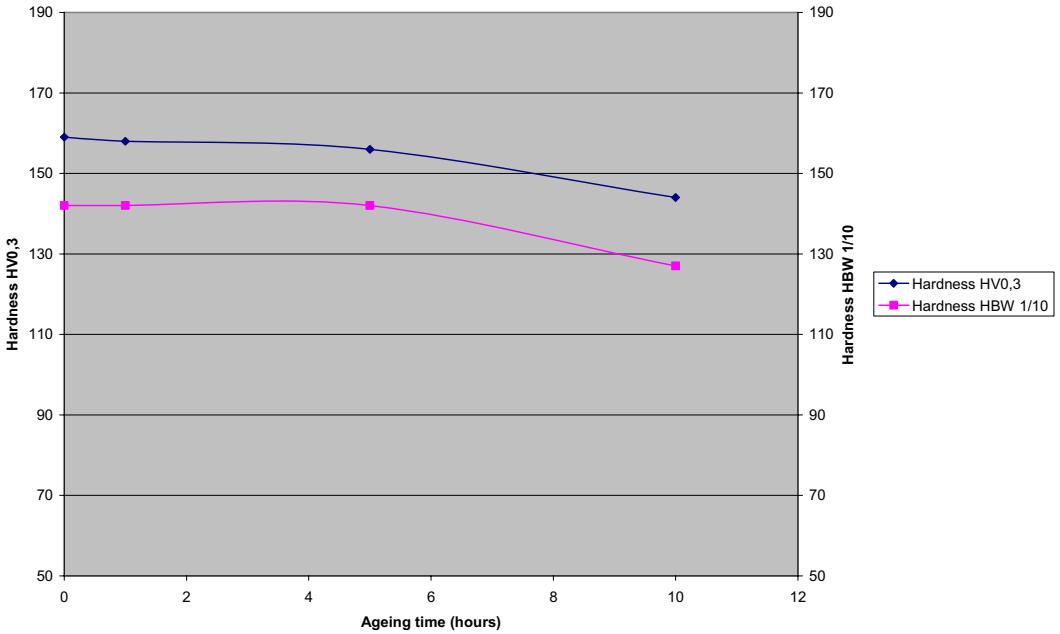

Fig. 9. Micro-hardness HV0.3 and hardness HBW 1/10 depending on the artificial ageing duration (160 °C).

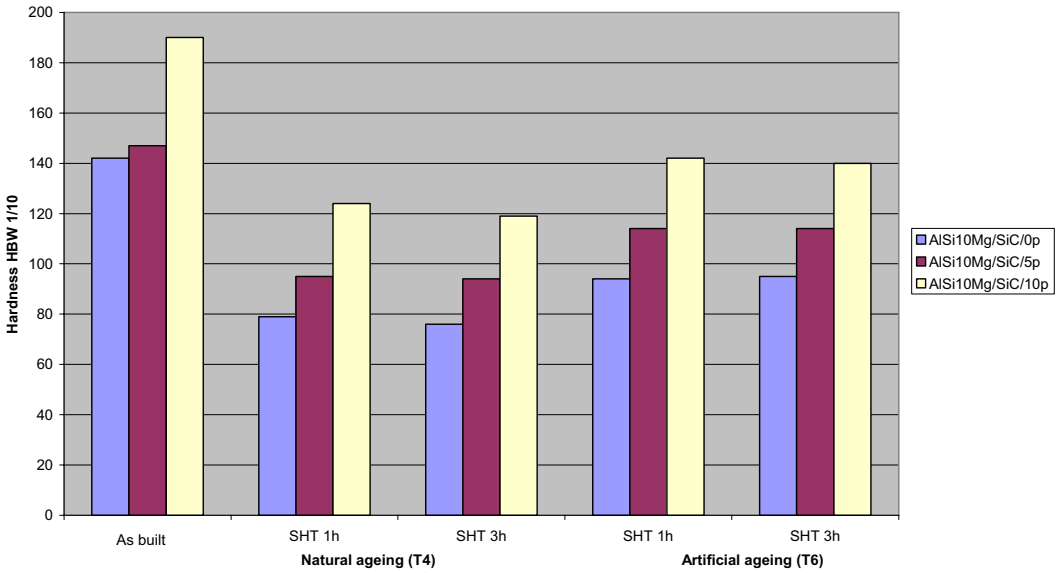

Fig. 10. Influence of the solution heat-treatment time on natural and artificial ageing (AlSi10Mg alloy and MMCs).
Note: natural ageing for at least 4 days, artificial ageing for 5 h at 160 °C.

Table 3. Hardness values of AlSi10Mg alloy and MMC depending on temper.

Alloys	Hardness HBW	Sources
AlSi10Mg (SLM) T6	95 (approximately)	In this study
AlSi10Mg KT6	90 mini	Table 2 – NF EN 1706 [8]
A-S10G Y33	95 (typical)	Aluminium Pechiney [13]
AlSi10Mg/SiC/10p-T6	140 (approximately)	In this study
F3S.10S T6	128 (typical)	Duralcan composites [15]

It is clear that the hardness of AlSi10Mg T6 alloy obtained from selective laser melting meets NF EN 1706, corresponding exactly to the data given by Aluminium Pechiney [13]. There is thus no improvement in the mechanical characteristics under such conditions.

At as-built temper, AlSi10Mg alloy from powder-bed fusion exhibits particularly high hardness values: much higher than both the temper F and T6 states given by NF EN 1706 [8]. It is also 30 HV above the values given by Kempen et al. [14] for a similar manufacturing technique.

AlSi10Mg/SiC/10p-T6 MMC from selective laser melting thus has a higher hardness than an equivalent commercial alloy such as F3S.10S T6 [15]. The hardness of the AlSi10Mg/SiC/10p-T6 is therefore improved by about 9–10%.

The electrical conductivity is often used to monitor the precipitation of an aluminium alloy.

Variations in the electrical conductivity of the AlSi10Mg alloy (from selective laser melting) were also monitored in relation to the artificial ageing duration (similarly to the hardness, as presented previously) (Fig. 11).

Electrical conductivity increases with artificial ageing time, implying an evolution of the alloy precipitation, and thus a modification of the mechanical properties. However, no changes in hardness were noted (Fig. 9). As such, despite a modification of the alloy precipitation, the latter does not seem to significantly influence as-built temper hardness.

Figure 12 shows the electrical conductivity in relation to various tempers; considering the conventional metallurgy of aluminium alloys, temper T4 exhibits lower electrical conductivity (along with a lower hardness) than T6. Note the electrical conductivity for a 3 h solution heat treatment is slightly under that for a 1 h one, regardless of the subsequent treatment stage (natural or artificial ageing). This is possibly due to a more efficient solution heat treatment for a 3 h long operation: more precipitates dissolve into the solid aluminium solution. However, if this difference exists, it has no significant effect on the hardness values.

Table 4. Young's modulus, *E* (AlSi10Mg alloy).

Sample No.	Density (kg.m^{-3})	*E* Modulus (MPa)
1	25 57	66 704
2	25 62	66 424
3	25 63	65 807
Average		66 312
Standard deviation		459

Table 5. Comparison of Young's modulus (AlSi10Mg alloy).

Alloy	*E* modulus (GPa)	Sources
AlSi10Mg-A359.0 Gravity permanent mould casting	72	[16]
AlSi10Mg SLM	68 ± 3	[14]
AlSi10Mg SLM	66.3 ± 0.5	In this study

2.2.4 Mechanical characteristics

2.2.4.1 Young's modulus

For these trials, three samples as per Section 1.3 were used. Table 4 presents the measured *E*-modulus, according to Equation (3).

The selected value for Young's modulus for AlSi10Mg alloy (from selective laser melting) is 66.3 ± 0.5 GPa. Comparison was made with values found in the literature, as presented in Table 5.

The measured value is 8% lower than that conventionally accepted in gravity permanent mould casting; however, compared with values obtained from a similar production method, the gap is smaller but still remains lower [14].

We also established Young's modulus for the AlSi10Mg/SiC/5p composite. Of all three samples available for this material, only one was retained; the others were too small and/or of too low density.

For the AlSi10Mg/SiC/5p MMC (from selective laser melting) the value for Young's modulus retained is 77.3 GPa. Young's modulus is therefore increased by approximately 16.5% compared with the AlSi10Mg alloy.

According to Totten [17], the rule of mixtures or the iso-deformation criteria are given by Equation (5) and the iso-stress criteria are given by Equation (6).

$$Ec_{\mathrm{d}} = Vm\,Em + Vp\,Ep \quad \text{(iso-deformation criteria)} \quad (5)$$

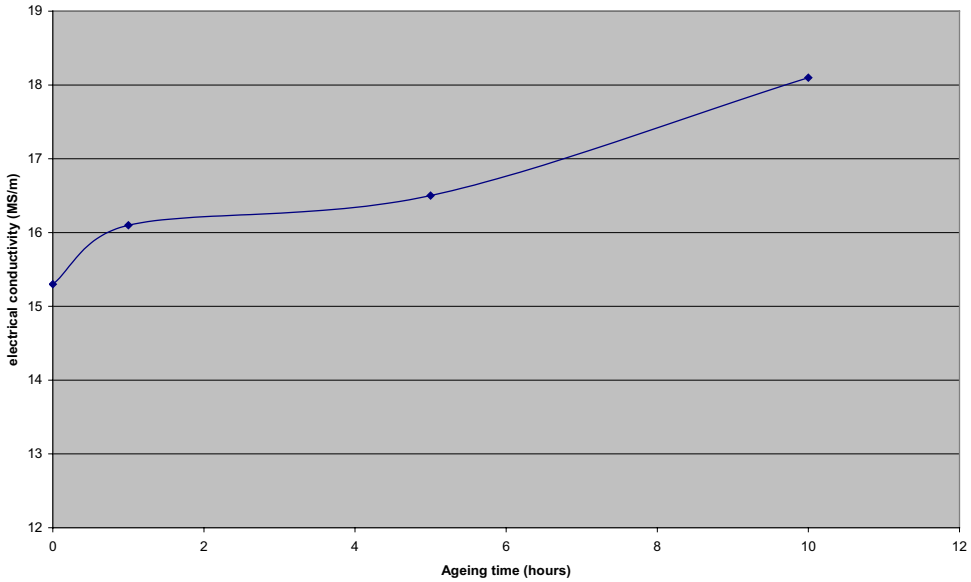

Fig. 11. Electrical conductivity depending on artificial ageing time (AlSi10Mg alloy).

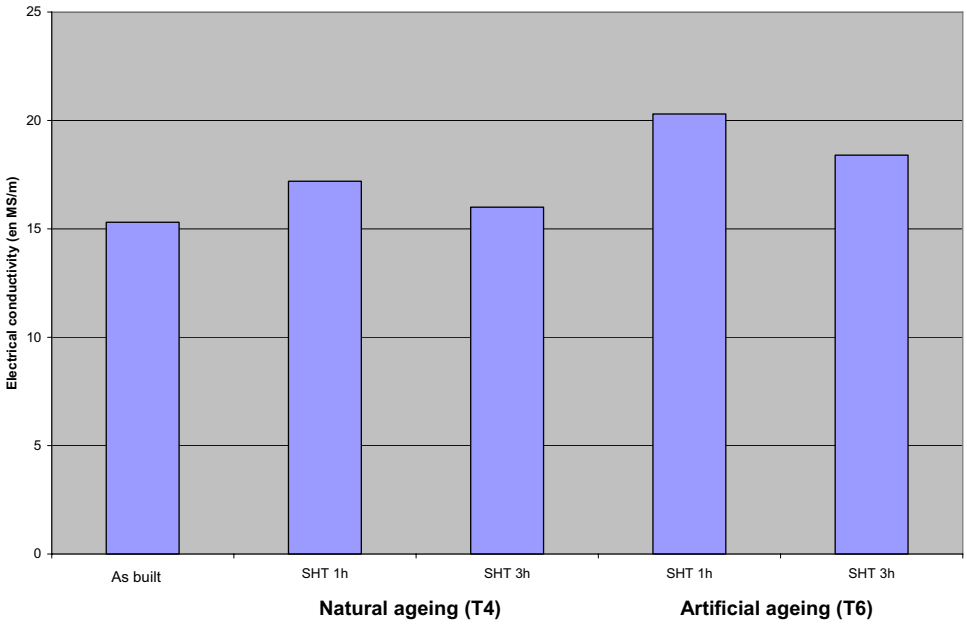

Fig. 12. Electrical conductivity depending on temper (AlSi10Mg alloy).

with:

- Ec_d or Ec_s (see Eq. (6)) the elasticity modulus for the composite;
- Em the elasticity modulus for the matrix;
- Ep the elasticity modulus for the particle reinforcement;
- Vm the matrix volume fraction;
- Vp the particle reinforcement volume fraction.

$$Ec_s = \frac{1}{\frac{Vm}{Em} + \frac{Vp}{Ep}} \text{ (iso-stress criteria)} \quad (6)$$

According to the literature [17], MMCs do not conform with the iso-deformation and iso-stress criteria. Indeed, aluminium alloy MMCs are between two laws: the iso-stress criteria being the lower limit and the iso-deformation criteria being the upper limit.

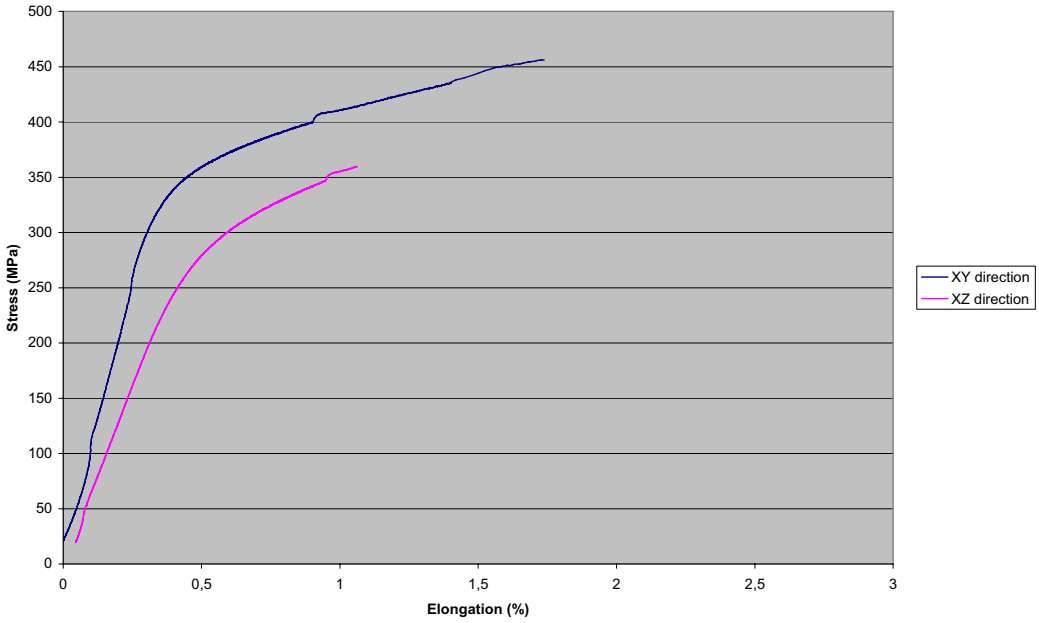

Fig. 13. Conventional tensile curves for AlSi10Mg alloy (as built) by selective laser melting.

Table 6. Conventional mechanical characteristics of AlSi10Mg alloy (SLM).

AlSi10Mg (as built)				
Orientation	Temperature	*Rm* (MPa)	$Rp_{0.2}$ (MPa)	*A* (%)
XY	Room temperature	456	368	3.0
XY	180 °C	348	253	3.3
Z	Room temperature	359,5	306,5	1.7
Z	180 °C	285	213	3.5
AlSi10Mg (Solution heat-treating + quenching + artificial ageing) (T6)				
Orientation	Temperature	*Rm* (MPa)	$Rp_{0.2}$ (MPa)	*A* (%)
XY	Room temperature	312	–	3.2
XY	180 °C	–	–	–
Z	Room temperature	290	262	2.5
Z	180 °C	251	198	2.6

In this case, the values obtained are E_{Cs} = 69.3 GPa and E_{Cd} = 87 GPa; as expected the *E* modulus for the AlSi10Mg/SiC/5p composite lies in this range.

2.2.4.2 *Conventional mechanical characteristics*

Two tempers are selected:

- As-built temper.
- Solution heat-treated (540 °C for 1 h) + quenching + artificial ageing (160 °C for 5 h) (temper T6).

Table 6 presents the mechanical properties of horizontally and vertically built tensile test samples for as-built AlSi10Mg and AlSi10Mg T6 material.

The as-built temper mechanical characteristics are systematically better, as previously suggested by the hardness measurements conducted. As expected, mechanical characteristics at 180 °C are lower than at ambient temperature. There is also a strong anisotropy of these characteristics, the latter being always higher in the (x, y) plane than in the *Z* direction, as shown in Figure 13.

Conversely, the paper from Kempen et al. [14] does not give any evidence of anisotropy, despite using the same production strategy for the alloy (Fig. 3 in Ref. [14]).

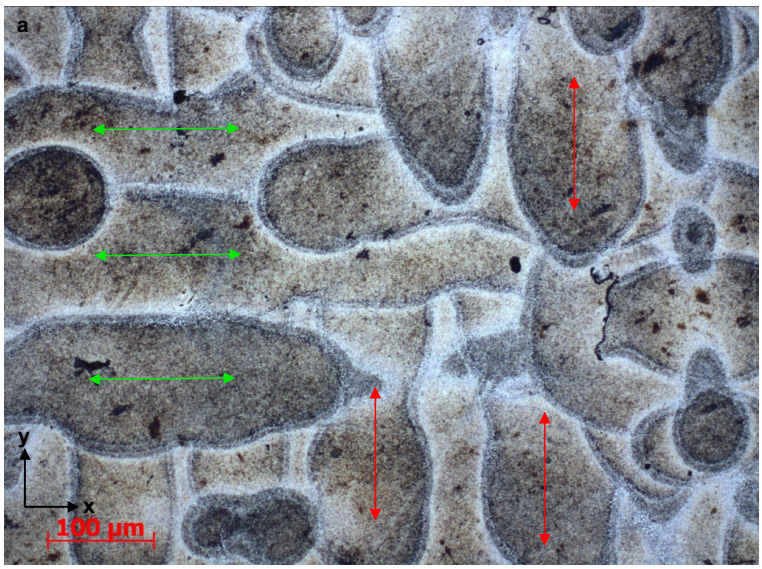

(a)

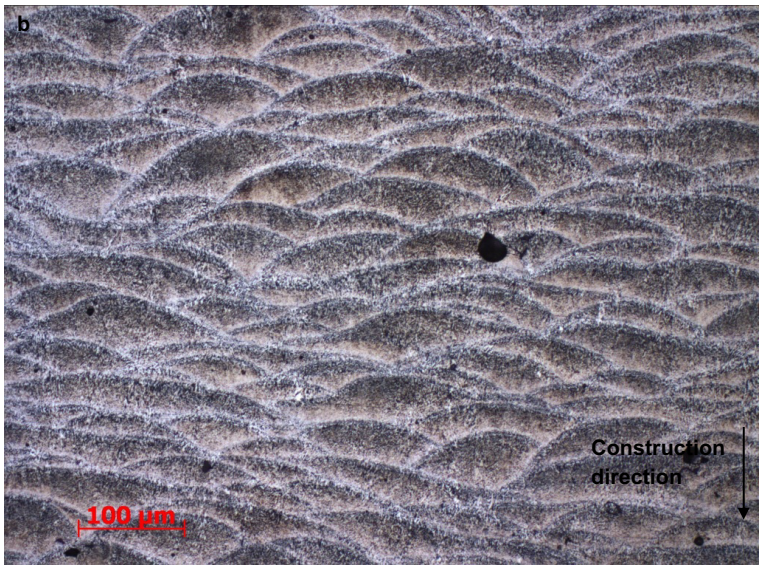

(b)

Fig. 14. (a) As-built AlSi10Mg, plane (x, y), (b) as-built AlSi10Mg, Z direction.

In the same paper, the mechanical characteristics (Rm) in plane (x, y) are 12% lower than the ones presented here.

2.2.5 Metallographic study

2.2.5.1 Construction strategy

As detailed in Setion 1.1, the manufacturing strategy is "crossed". On pins under a microscope, this strategy is defined by tracks oriented at 0° and 90° (Figs. 14a and 14b) in plane (x, y) along with "waves" representing track segments in planes (x, z) or (y, z) [18].

The observations of Figure 14 performed on the AlSi10Mg alloy are also valid for MMCs.

Note that building tracks are clearly drawn by their contour, appearing entirely homogeneous.

2.2.5.2 Microstructure

In Figure 15 showing the optical microscope results, the following are seen.

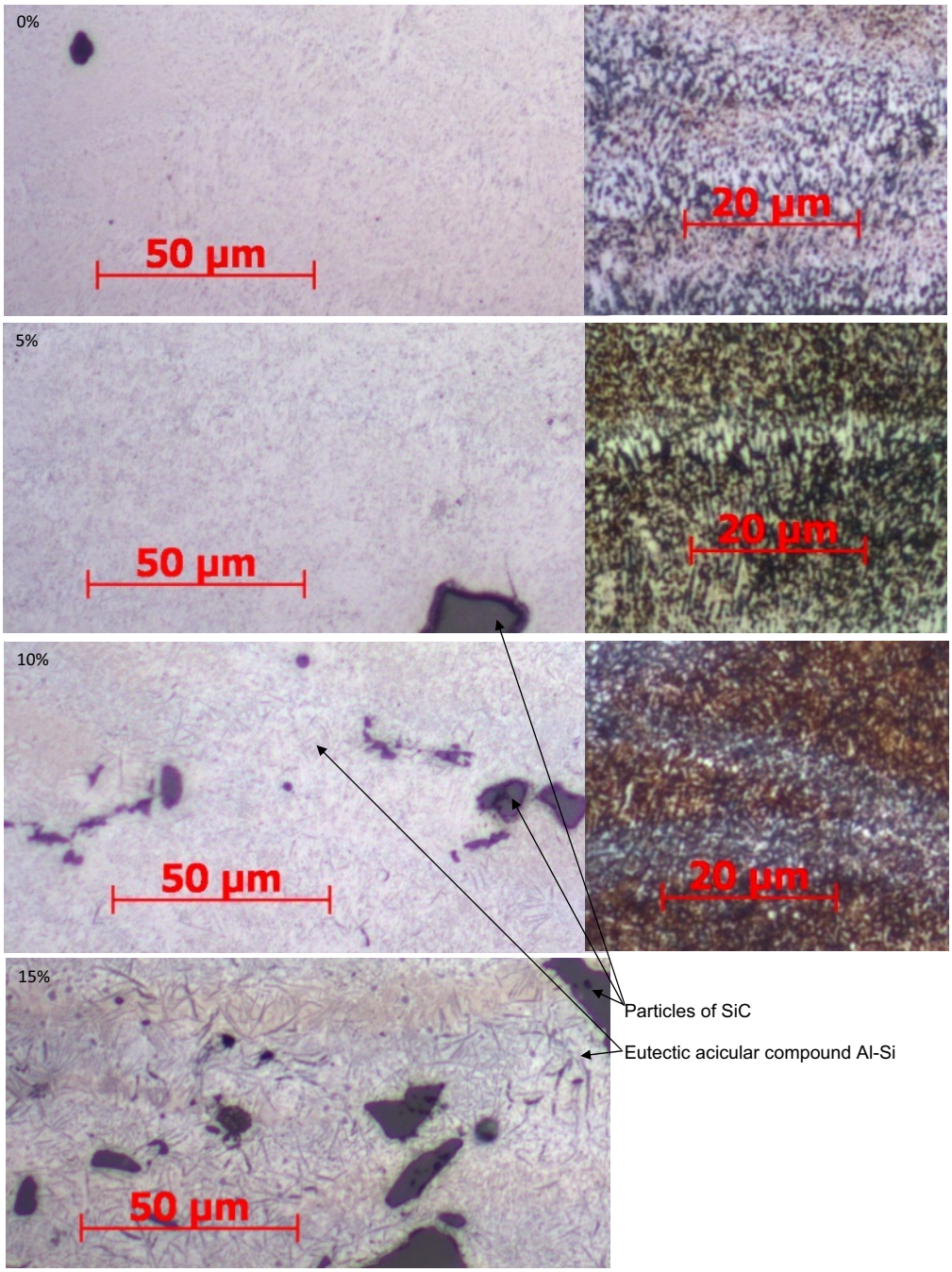

Fig. 15. Microscopic results without and with etching (reagent with sulphuric acid) of: 0% AlSi10Mg/SiC/0p – 5% AlSi10Mg/SiC/5p – 10% AlSi10Mg/SiC/10p – 15% AlSi10Mg/SiC/15p (no etching).

The microstructure of all the materials (Fig. 15) is made of dendrites (more or less fine) of solid aluminium solution along with acicular Al-Si eutectics. Nevertheless the microstructure rapidly evolves: an increase in the reinforcements (SiC) volume fraction modifies the latter to a "coarser" one. It is then characterised by the increased presence of acicular components (mainly Al-Si eutectics) with the increase in the reinforcement volume fraction.

The grains are not revealed here. Only electrolytic etching can reveal them. We will see that they have a size of a few tens of

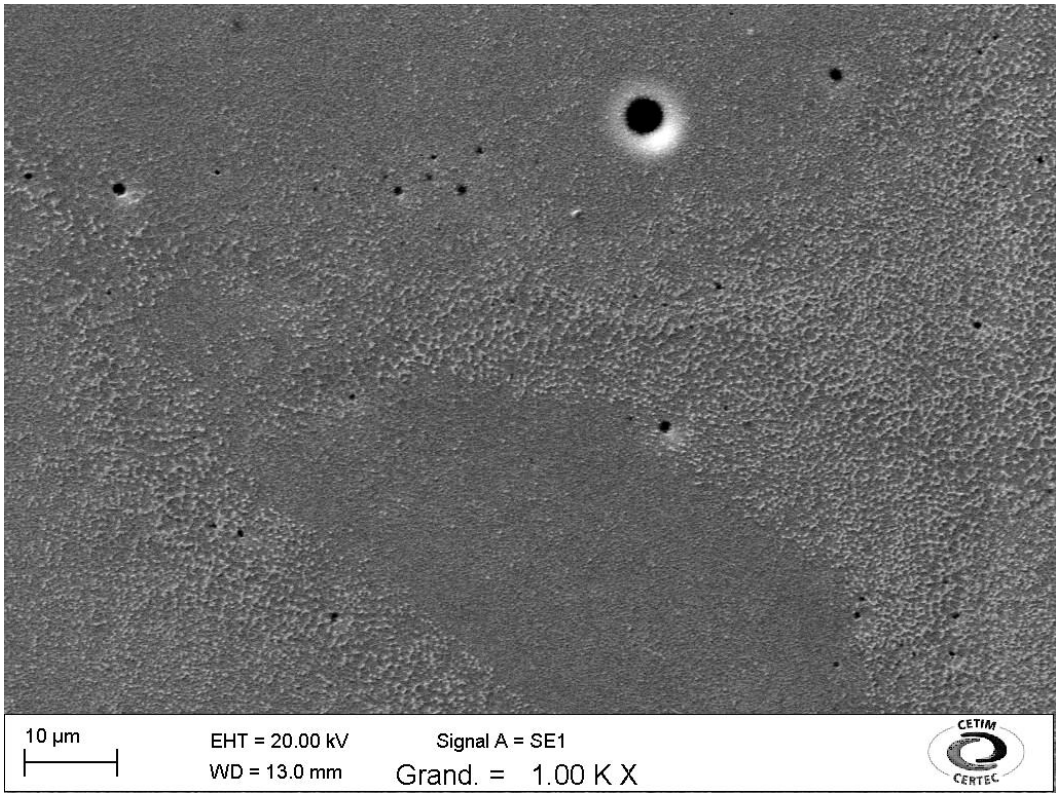

Fig. 16. As-built AlSi10Mg alloy- SEM.

micrometres (Figs. 21 and 22). The grain is defined as the group consisting of the dendrite and the eutectic.

Moreover, construction tracks are more distinguishable on micrographics with etching (reagent with sulphuric acid) (Fig. 15). The dendrite structure, along with its Al-Si eutectics, is more clearly seen; in particular, it appears there is an orientation of both dendrites and eutectic components that was not noted on the micrographics without etching. This orientation can only be seen for AlSi10Mg alloy and for AlSi10Mg/SiC/5p (stated 5%) MMC.

2.2.5.3 Track contour

As seen in Figure 14, contours for tracks obtained through selective laser melting are clearly spotted and appear to be of a coarser structure than the track core. The following figure (Fig. 16) shows AlSi10Mg tracks under the SEM; the coarse structure of the track contours is clearly visible.

Generating an X-ray map (using the EDS on the SEM) of the same area (Fig. 17), a higher concentration of the element Si can be found in the track contours (specifically on the coarser structures).

Other main elements (namely Mg) are well spread, with no specific positioning.

It appears that higher concentrations of Si-made eutectic are located around the tracks (in the coarser structures). Looking closely at the track contours, there is indeed a zone of coarser structure approximately 8–9 μm wide. This zone is delimited on one side by the fine structure of the track core (No. 1 in Fig. 18) previously constructed, and by the fine structure on the outer edge of the newly constructed track (No. 2 in Fig. 18) on the other side.

An even coarser structure concentrated in a lane located in the altered structure area can be seen in Figure 19. This lane most likely separates the heat-affected zone within a previously manufactured track (1). It is approximately 2 μm thick; it is thus the most affected in terms of structural changes ("coarse"), being closest to the liquid metal for the newly constructed track (2). A smaller

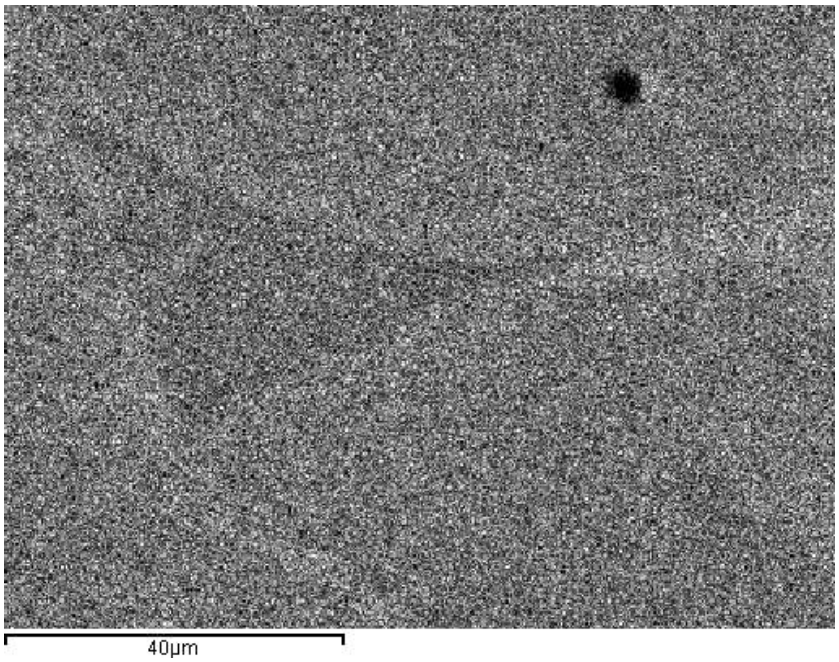

Fig. 17. Element Si (white) evidences.

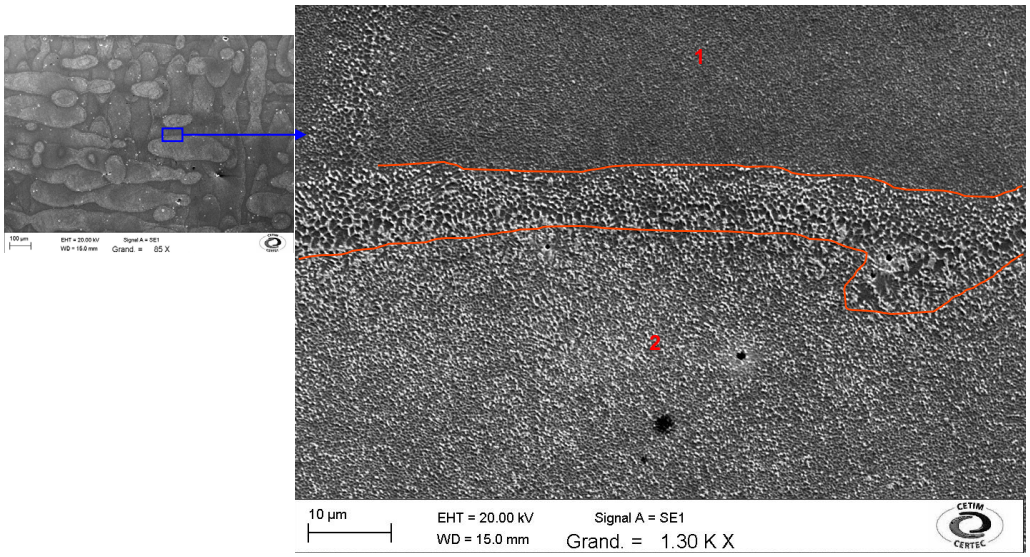

Fig. 18. Building track contour.

"disturbed" area is also found in the new track, which may be caused by several factors: a dough-like area, modified cooling rate, etc.

2.2.5.4 Grain size and DAS (AlSi10Mg alloy)

The DAS (dendrite arm spacing) is the distance between secondary arms and dendrites (of aluminium alloy solid solution). In recent years, DAS has been used to describe the metallurgical structure of cast alloys and to estimate their mechanical characteristics [1]. In Figure 20, fine dendrites of solid aluminium solution along with Al-Si eutectics are observed. The DAS for the AlSi10Mg alloy is evaluated at 0.5–0.6 μm (Table 7 and Fig. 20) with the intercept method [19].

These observations confirm that the structure obtained by additive

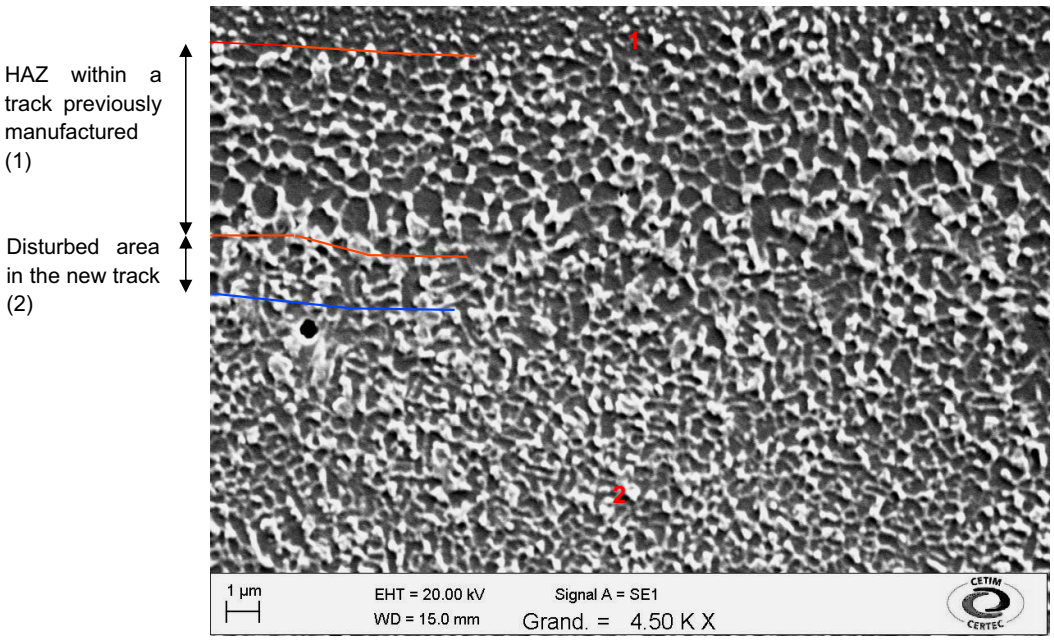

Fig. 19. Details of a building track contour: HAZ and disturbed area.

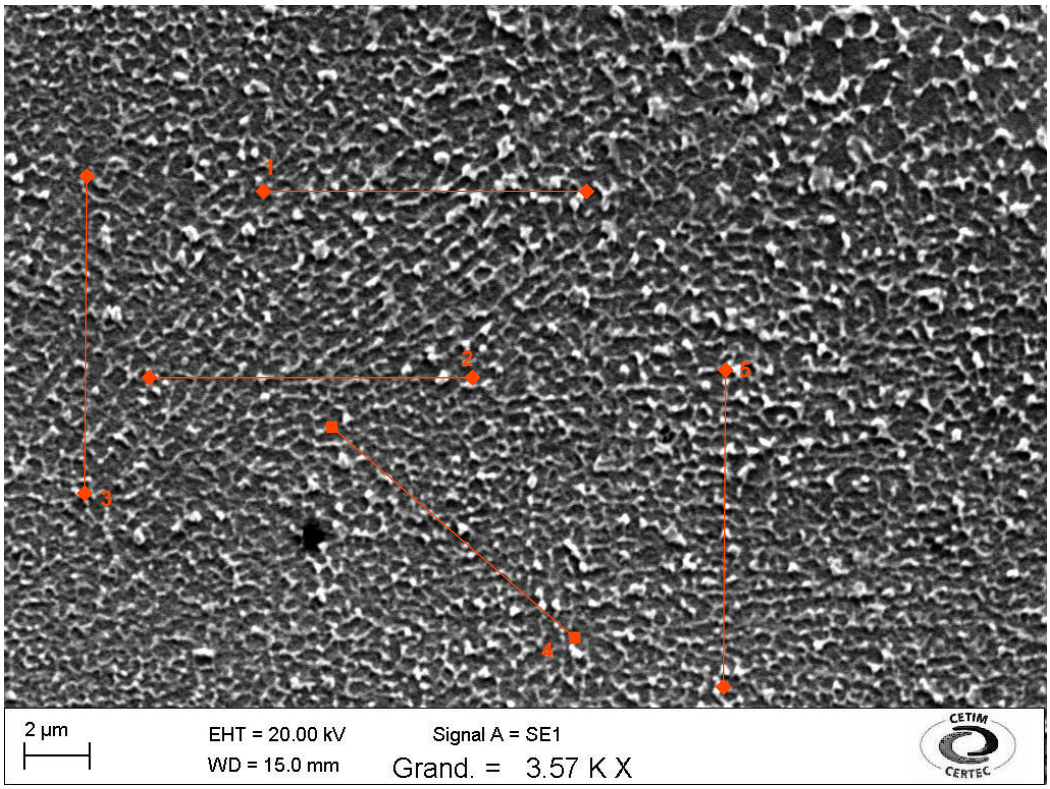

Fig. 20. Practical application of the intercept method – AlSi10Mg alloy (example).

Table 7. DAS measurement.

Line (Fig. 20)	Number of dendrite intercepted	Line length (μm)	DAS (μm)
1	16	10	0.63
2	18	10	0.56
3	21	10	0.48
4	20	10	0.50
5	21	10	0.48

manufacturing (selective laser melting) is rather fine. Indeed, the DAS for good quality gravity permanent mould casting is of the order of 20 μm [19].

The Hall-Petch [20] law relates the DAS size to the mechanical characteristics (yield strength $Rp_{0.2}$) as follows:

$$Rp_{0.2} = A + \frac{K}{\sqrt{DAS}} \tag{7}$$

A hardening effect (increase in the yield strength) $\Delta Rp_{0.2}$ can be expressed as in Equation (8); hardening is obtained by the dendrites refinement, for which the mean DAS value goes from DAS_1 to DAS_2 ($DAS_1 < DAS_2$):

$$\Delta Rp_{0.2} = K\left(\frac{1}{\sqrt{DAS_2}} - \frac{1}{\sqrt{DAS_1}}\right) \tag{8}$$

The coefficient K is dependent on the metal, more specifically its crystalline system; as such, the $\Delta Rp_{0.2}$ is in MPa, the DAS in mm and K is of the order of 8 for aluminium alloys [23].

Thus, going from $DAS_1 = 20$ μm to $DAS_2 = 0.5$–0.6 μm, the hardening is valued at 270 MPa. Referring to the expected yield strength of AlSi10Mg alloy from gravity permanent mould casting in temper F (e.g. 100–110 MPa) and the yield strength obtained from selective laser melting, in as-built samples (e.g. 365 MPa, see Sect. 2.2.4.2, Table 6), the value found is $\Delta Rp_{0.2} = 260$ MPa (approximately). The Hall-Petch relation thus appears to clarify the increase in mechanical properties generated from selective laser melting.

The microstructure size obtained is dependent on the cooling rate v. The following relation is often found in reference [23]:

$$\lambda = Bv^{-n} \tag{9}$$

with:

- λ the formed grain size (or distance between dendrite arms);
- B and n constants, dependent on the alloy considered.

For Al-Si alloys λ is assimilated to the DAS in Equation (9), thus giving:

$$DAS = \frac{B}{\sqrt[3]{v}} \tag{10}$$

Thus

$$v = \left(\frac{B}{DAS}\right)^3 \tag{11}$$

Taking $B = 35$, $n = 1/3$ and $DAS = 0.6$ μm [23], the cooling speed is 200 000 °C.s^{-1}, which corresponds to the admissible cooling speed for selective laser melting [24].

Another technique to assess the cooling rate is the resolution of the heat equation in three-dimensional space (x, y, z). Only one numerical solution of the equation that we have not implemented here is conceivable.

The following figure (Figs. 21a and 21b) shows alloy grains located inside building tracks on an (x, z) and (x, y) cut.

The grains are oriented along Z with the tracks; there is thus a strong grain size anisotropy in the Z direction in the (x, y) plane. Indeed, grain size ranges from 1 to 10 μm in plane (x, y) whilst ranging from 17 to 42 μm along Z. As before, this yield strength anisotropy (between plane (x, y) and the Z direction) may be explained through the Hall-Petch law. Replacing the DAS by the grain size (mean diameter) gives:

$$\Delta Rp_{0.2} = K\left(\frac{1}{\sqrt{d_2}} - \frac{1}{\sqrt{d_1}}\right) \tag{12}$$

with $d_2 \approx 5$ μm and $d_1 \approx 30$ μm, the value found is $\Delta Rp_{0.2} = 67$ MPa (approximately). In this study, $\Delta Rp_{0.2}$ (anisotropy) ≈62 MPa, thus showing the accuracy of the Hall-Petch law.

The following figure (Fig. 22) shows the grain orientation within the track into a cut (x, z). It appears that the grains grow from the edges of the bead in contact with other building tracks to the outer surface of the bead (in contact with argon): this is simply due to a directional solidification: faster cooling at the surface of already consolidated material.

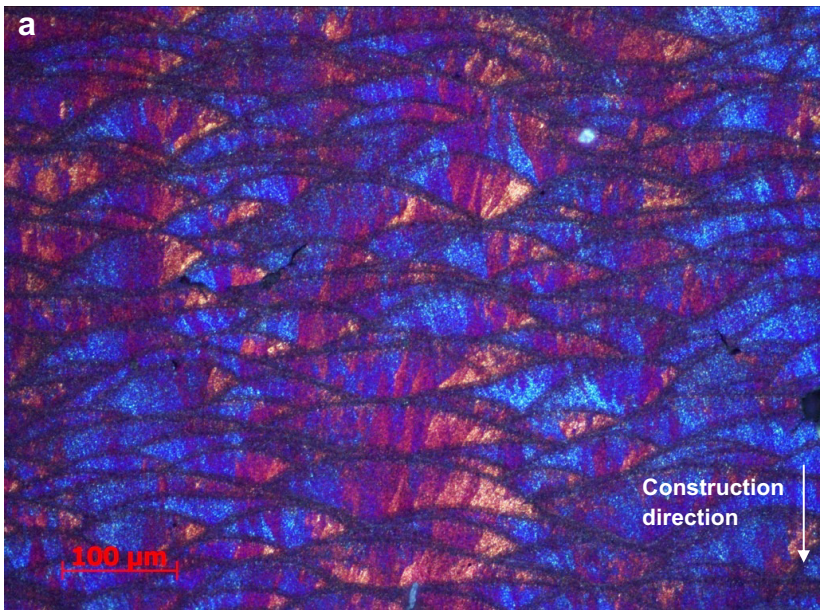

(a)

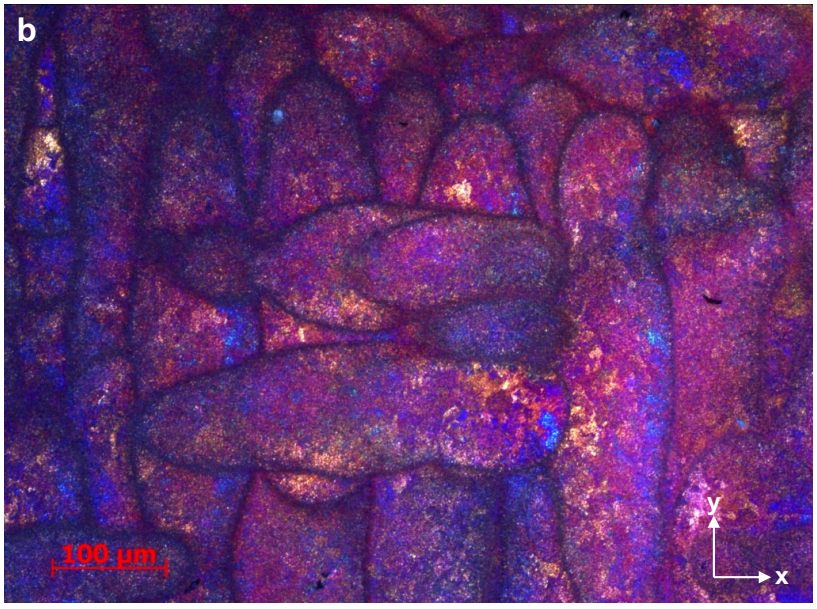

(b)

Fig. 21. (a) Grain exposure in tracks via electrolytic etching: plane (x, z), (b) grain exposure in tracks via electrolytic etching: plane (x, y).

Note also in Figure 22, the almost identical grain orientation within manufacturing tracks.

2.2.5.5 *Structural modification after heat treating*

When performing a solution treatment-quenching-artificial ageing (say for temper T6 – see Sect. 1.4) on as-built AlSi10Mg pins made by selective laser melting, the alloy structure is modified. Comparing Figures 21 (as built) and 23 (after heat treatments):

- The suppression of building tracks [21].
- A more random grain orientation [21].
- A grain size ranging from 16 to 42 μm.

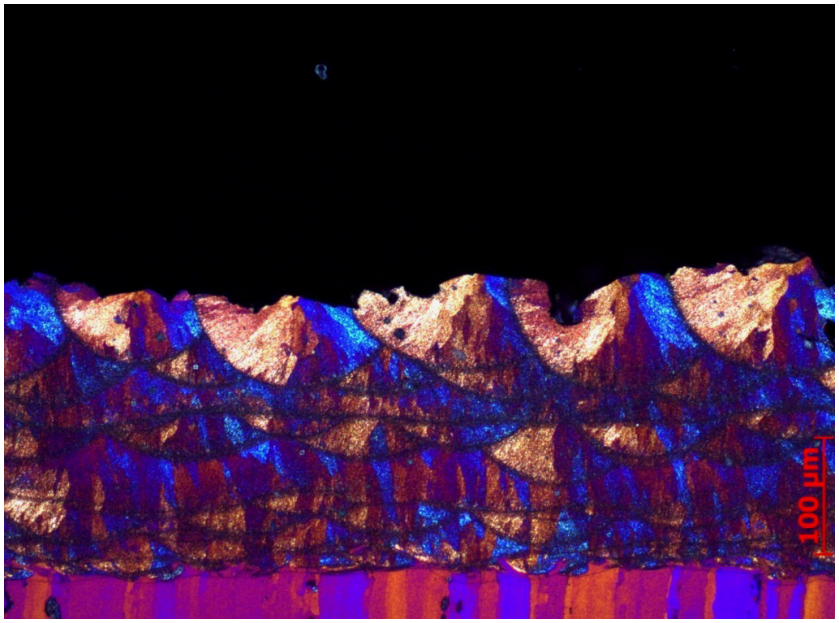

Fig. 22. Demonstration of the grain growth within a track (electrolytic etching).

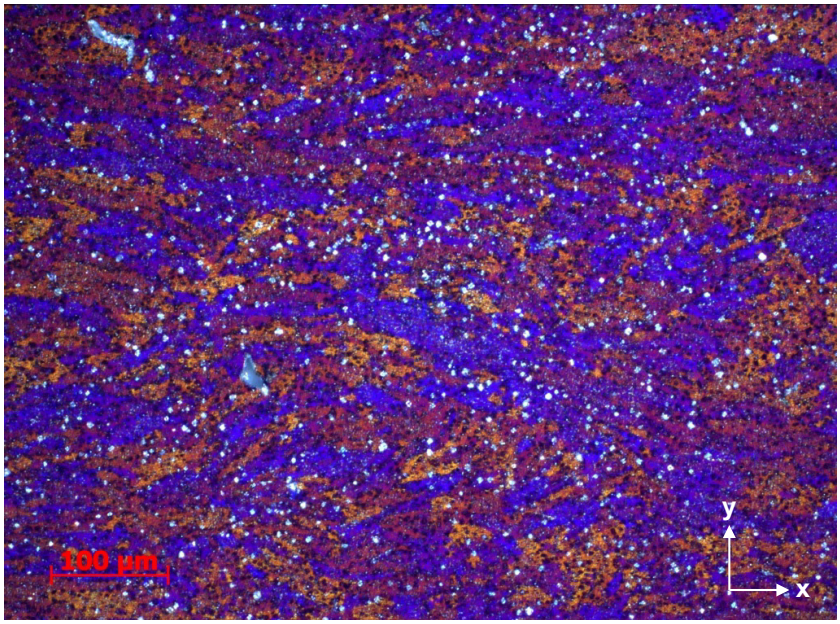

Fig. 23. Grain exposure after heat treatment, obtained via electrolytic etching.

Figure 24 clearly shows the thin dendrites of solid aluminium solution along with Al-Si eutectics have been removed. In their stead, a solid aluminium solution matrix is formed, with polyhedron Si crystals (of 0.5–4 μm). It appears that Al-Si eutectic is broken down into solid aluminium solution and Si crystals. The latter is rather surprising, given that the solution heat-treatment temperature (540 °C) is not sufficient to obtain a priori Si crystals.

This new structure does not seem to be in favour of hardness (or mechanical characteristics) since the latter significantly drop (Sect. 2.2.3). The temper T6 hardness is, however, as expected for the cast (e.g. gravity permanent mould casting) though the structures are not similar.

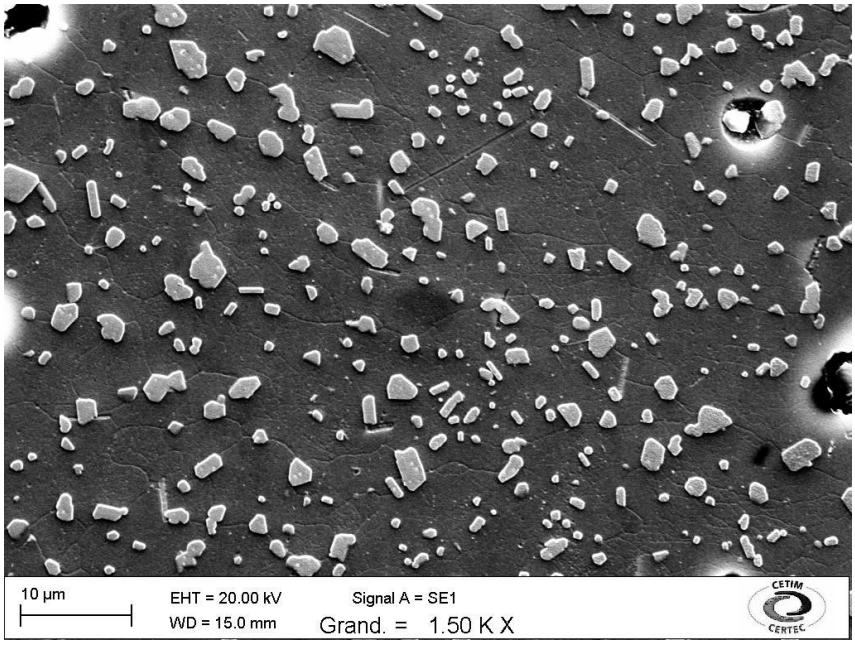

Fig. 24. AlSi10Mg alloy (selective laser melting) microstructure T6.

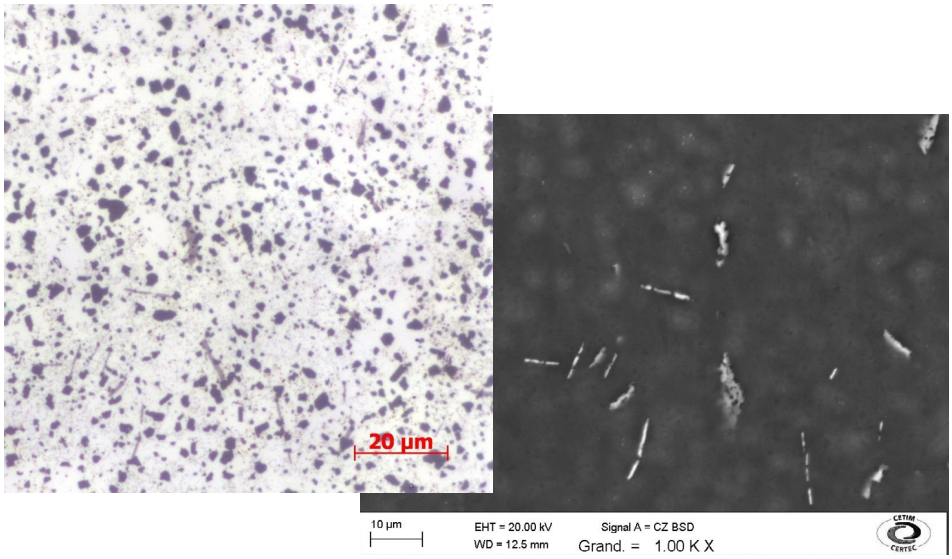

Fig. 25. Optical microscope and SEM observation of Al-Si-Fe precipitates.

Additionally, along with the structural changes previously revealed (also found in Fig. 25), Al-Si-Fe precipitates also appeared (possibly $FeSiAl_5$ plates).

These precipitates are not found in the as-built samples (selective laser melting). It is possible that these precipitates are dissolved (in the solid aluminium solution) at higher temperatures (beyond the solution heat-treatment temperature), and thus not precipitating because of the high cooling speed.

3 Conclusion

The study of additive processing of AlSi10Mg aluminium alloy and MMCs obtained from selective laser melting shows:

– The difficulty of manufacturing MMC samples from 15% (in volume) SiC

reinforcements, probably due to residual stresses.
- The temperature reached by the laser beam appears to cause vaporisation of metals with low evaporation point, such as magnesium (or zinc in other aluminium alloys).
- When the volume fraction of SiC reinforcements increases, there is an evolution of the microstructure, with the appearance of acicular components.
- Higher mechanical properties for the as-built temper, associated with F (as manufactured) or T1 according to the normalization in place (i.e. cooled after heat transformation and natural ageing until stabilised).
- Significant increase in the conventional mechanical properties compared with casting, due to hardening by structure refinement. This effect can be described by the Hall-Petch law, and is linked to a rapid cooling rate of approximately 200 000 °C/s.
- Surprising changes in the alloy metallurgical structure caused by the heat treatments (solution treating-quenching-artificial ageing): a solid aluminium solution matrix with polyhedron Si crystals and Al-Si-Fe precipitates (possibly $FeSiAl_5$ plates).

Acknowledgements

The authors would like to thank the CETIM (Centre Technique des Industries de la Mécanique) for the financing and support provided for this study.

References

[1] Technique de l'ingénieur M4675, JACOB Sylvain, Propriétés des alliages d'aluminium de fonderie

[2] norme NF EN ISO 6892-1 et -2, Matériaux métalliques – Essais de traction – Partie 1: méthode d'essai à température ambiante – Partie 2: Méthode d'essai à température élevée

[3] standard SAE aerospace AMS2772E, Heat treatment of aluminum alloy raw materials

[4] A.B. Spierings, M. Schneider, R. Eggenberger, *Rapid Prototyping J.* **17** (2011) 380-386

[5] A. Renault, Caractérisation mécanique dynamique de matériaux poro-visco-élastiques, Thèse de doctorat, Université de Sherbrooke, département de génie mécanique, 2008, 149 p.

[6] norme NF EN ISO 6506, Matériaux métalliques – Essai de dureté Brinell

[7] norme NF EN ISO 6507, Matériaux métalliques – Essai de dureté Vickers

[8] norme NF EN 1706, Aluminium et alliages d'aluminium – Pièces moulées – Composition chimique et caractéristiques mécaniques

[9] L. Dembinski, Enjeux industriels en mécanique : de l'impression 3D à la fusion laser, Principe et élaboration de poudre par atomisation gazeuse, granulométrie et traçabilité pour la fabrication additive, Rendez vous technologique du CETIM-CERTEC, octobre 2013

[10] F.X. Tissot, Étude phénoménologique et modélisation du comportement du bain de fusion en soudage TIG en vue d'une application au contrôle du procédé, Rapport CEA, Saclay, 1998, 184 p.

[11] G. Tirand, Étude des conditions de soudage laser d'alliages base aluminium par voie expérimentale et à l'aide d'une simulation numérique, Thèse de doctorat, École doctorale des sciences physiques pour l'ingénieur, Bordeaux, 2012, 131 p.

[12] EOS aluminium AlSi10Mg, Material data sheet, may 2014, 5 p

[13] Division alliages de moulage, Les alliages d'aluminium de fonderie, Aluminium Pechiney, France, 1991

[14] K. Kempen, L. Thijs, J. VaN Humbeeck, J.P. Kruth, *Phys. Proc.* **39** (2012) 439-436

[15] Duralcan composites for gravity casting, Property data, Alcan

[16] ASM International Handbook commitee, Aluminium and aluminium alloys, 3rd edition. J.R. Davis, USA, 1996, 784 p.

[17] G. Totten, S. Mac Kenzie, Handbook of Aluminum, Marcel DEKKER, New York, 2003, Vol. 2, 1296 p.

[18] K. Kempen, L. Thijs, E. Yasa, M. Bradrossamay, W. Verheecke, J.P. Kruth, Process optimization and microstructural analysis for selective laser melting of AlSi10Mg

[19] B. Zhang, M. Garro, C. Tagliano, *Metall. Sci. Technol.* **21** (2003) 1

[20] Technique de l'ingénieur M230. CHENAL Bruno, DRIVER Julian, Ecrouissage d'alliages d'aluminium

[21] G. Murry, Aide mémoire métallurgie : Métaux – alliages – propriétés, Dunod, Paris, 2004

[22] J. Colbert Caractérisation de la fraction solide dans les lopins semi-solides produits par le procédé SEED, Mémoire maîtrise en ingénierie, Université du Québec, Chicoutimi, 2007, 239 p.

[23] M. Averyanova, Fusion laser de poudres métalliques : maîtrise du procédé pour la fabrication directe de pièces mécaniques, Thèse de doctorat, École nationale d'ingénieur de Saint Etienne, Saint Etienne, 2011, 236 p.

[24] E. Brandl, U. Heckenberger, V. Holzinger, D. Buchbinder, *Mater. design* **34** (2012) 159-169